

**Anomalous change of the magnetic moment direction by hole doping in CeRu<sub>2</sub>Al<sub>10</sub>**A. Bhattacharyya,<sup>1,2,\*</sup> D. D. Khalyavin,<sup>1,†</sup> D. T. Adroja,<sup>1,2,‡</sup> A. M. Strydom,<sup>2</sup> A. D. Hillier,<sup>1</sup>  
P. Manuel,<sup>1</sup> T. Takabatake,<sup>3</sup> J. W. Taylor,<sup>1</sup> and C. Ritter<sup>4</sup><sup>1</sup>*ISIS Facility, Rutherford Appleton Laboratory, Chilton, Didcot, Oxon OX11 0QX, United Kingdom*<sup>2</sup>*Highly Correlated Matter Research Group, Physics Department, University of Johannesburg, Auckland Park 2006, South Africa*<sup>3</sup>*Department of Quantum Matter, ADSM and IAMR, Hiroshima University, Higashi-Hiroshima 739-8530, Japan*<sup>4</sup>*Institut Laue Langevin, 6 rue Jules Horowitz, 38042 Grenoble, France*

(Received 29 August 2014; revised manuscript received 21 October 2014; published 11 November 2014)

We present a detailed investigation of the hole (3% Re) doping effect on the polycrystalline CeRu<sub>2</sub>Al<sub>10</sub> sample by magnetization, heat capacity, resistivity, muon spin relaxation ( $\mu$ SR), and neutron scattering (both elastic and inelastic) measurements. CeRu<sub>2</sub>Al<sub>10</sub> is an exceptional cerium compound with an unusually high Néel temperature of 27 K. Here we study the stability of the unusual magnetic order by means of controlled doping, and we uncover further surprising attributes of this phase transition. The heat capacity, resistivity, and  $\mu$ SR measurements reveal an onset of magnetic ordering below 23 K, while a broad peak at 31 K (i.e., above  $T_N$ ) has been observed in the temperature dependent susceptibility, indicating an opening of a spin gap above  $T_N$ . Our important finding, from the neutron diffraction, is that the compound orders antiferromagnetically with a propagation vector  $\mathbf{k} = (1,0,0)$  and the ordered state moment is  $0.20(1) \mu_B$  along the  $b$  axis. This is in sharp contrast to the undoped compound, which shows AFM ordering at 27 K with the ordered moment of  $0.34\text{--}0.42 \mu_B$  along the  $c$  axis. Similar to CeRu<sub>2</sub>Al<sub>10</sub> our inelastic neutron scattering study on the Re-doped compound shows a sharp spin gap-type excitation near 8 meV at 5 K, but with slightly reduced intensity compared to the undoped compound. Further the excitation broadens and shifts to lower energy ( $\leq 4$  meV) near 35 K. These results suggest that the low temperature magnetic properties of the hole-doped sample are governed by the competition between the anisotropic hybridization effect and the crystal field anisotropy as observed in hole-doped CeOs<sub>2</sub>Al<sub>10</sub>.

DOI: [10.1103/PhysRevB.90.174412](https://doi.org/10.1103/PhysRevB.90.174412)

PACS number(s): 61.05.fm, 75.30.Mb, 76.75.+i, 25.40.Fq

**I. INTRODUCTION**

The Kondo insulators (KI) belong to the class of strongly correlated materials forming a group of either nonmagnetic semiconductors (i.e., FeSb<sub>2</sub>) with the narrowest energy gap ( $\Delta$  in the Kelvin range) or of semimetals (e.g., CeNiSn, Ce<sub>3</sub>Bi<sub>4</sub>Pt<sub>3</sub>, SmB<sub>6</sub>, and YbB<sub>12</sub>), both with a heavy-fermion metallic state setting in at elevated temperatures  $T \geq \Delta$  [1–8]. The gaps inferred from optical, magnetic, transport, and thermodynamics properties are almost an order of magnitude smaller than those obtained by band structure calculations, which are due to the presence of strong electronic correlations [9,10]. As a consequence of a strong  $c$ - $f$  hybridization and the formation of a Kondo singlet ground state the Kondo insulating ground state is not compatible with magnetic ordering. Very recently the metal-insulator transition and surprisingly high temperature of magnetic phase transition ( $\sim 27$  K) in the orthorhombic Ce based cage type materials CeT<sub>2</sub>Al<sub>10</sub> (T = Os and Ru) have attracted considerable attention both experimentally and theoretically [11,12]. Antiferromagnetic (AFM) ordering of these Ce compounds is found at higher temperatures than in the isostructural Gadolinium compounds which rules out that the magnetic order is triggered by simple Ruderman-Kittel-Kasuya-Yosida (RKKY) type interactions. This suggests that a novel mechanism has to be formulated for the AFM order that exists in CeT<sub>2</sub>Al<sub>10</sub>.

The unusual magnetic phase transition in CeRu<sub>2</sub>Al<sub>10</sub> is discerned in the temperature dependence of several physical quan-

ties [11,13]. Resistivity, heat capacity, and the thermal conductivity measurements suggest that the transition may be accounted for by the formation of a charge-density wave (CDW) or spin-density wave (SDW), which opens an energy gap over a portion of the Fermi surface [11–14]. Furthermore the spin gap formation in CeRu<sub>2</sub>Al<sub>10</sub> has been confirmed through inelastic neutron scattering ( $\Delta = 8$  meV) [12,15,16], optical study ( $\Delta \sim 40$  meV) [17], and x-ray photoelectron spectroscopy ( $\Delta \sim 58$  meV) [18]. For CeRu<sub>2</sub>Al<sub>10</sub> the magnetic structure reported by Khalyavin *et al.* with a propagation vector of  $\mathbf{k} = (1,0,0)$  involves a collinear antiferromagnetic alignment of the Ce moments along the  $c$  axis of the orthorhombic  $Cmcm$  space group with a reduced moment of  $0.34(2) \mu_B$  [19]. A slightly bigger moment of  $0.42(1) \mu_B$  has been found in the study of CeRu<sub>2</sub>Al<sub>10</sub> single crystal by Kato *et al.* [20]. The moment direction is not governed by the single ion crystal electric field (CEF) anisotropy, which would align the moment along the easy  $a$  axis, having the highest susceptibility [21], but instead by the anisotropic hybridization [19]. This is a very unusual characteristic of the magnetic ordering in CeRu<sub>2</sub>Al<sub>10</sub>, because in local-moment rare earth magnetism the single-ion model is a standard and well-proven approach in the quantitative treatment of crystal electric fields and magnetocrystalline anisotropy prevailing in these materials. In noncubic Kondo insulators, the fascinating ground states emerging from extreme anisotropic hybridization is a topic of current interest [22]. The lightly hole-doped system CeOs<sub>1.96</sub>Re<sub>0.06</sub>Al<sub>10</sub> exhibits antiferromagnetic ordering of the Ce moments below  $T_N = 21$  K. The ordered moments are substantially reduced ( $0.18 \mu_B$ ) but preserve the anomalous direction along the  $c$  axis, indicating the important role of the  $c$ - $f$  hybridization in the anisotropic nature of the exchange interactions [23].

\*amitava.bhattacharyya@stfc.ac.uk

†dmitry.khalyavin@stfc.ac.uk

‡devashibhai.adroja@stfc.ac.uk

In the present work, we have investigated the marked change in the physical properties of  $\text{CeRu}_2\text{Al}_{10}$  induced by a small amount of hole (3% Re,  $\text{CeRu}_{1.94}\text{Re}_{0.06}\text{Al}_{10}$ ) doping using magnetization, resistivity, heat capacity, muon-spin relaxation, powder neutron diffraction, and inelastic neutron scattering measurements. The observation of magnetic Bragg peaks below 23 K in the neutron diffraction data and the independent observation of coherent oscillations due to an internal field in the time dependence of the longitudinal muon-spin relaxation spectra confirms the magnetic origin of the transition. Surprisingly, the refinements of the neutron diffraction data show that the best model corresponds to an AFM order of the Ce moment along the  $b$  axis of the  $Cmcm$  space group with an ordered state moment of  $0.20(1)\mu_B$  at 1.5 K. The inelastic neutron scattering study reveal the presence of a spin gap of 8 meV at 5 K, indicating that aside from the change in ordered moment direction and its magnitude found here in our analyses, all other attributes of the order parameter are retained in the doped compound  $\text{CeRu}_{1.94}\text{Re}_{0.06}\text{Al}_{10}$  compared to the stoichiometric  $\text{CeRu}_2\text{Al}_{10}$  [19].

## II. EXPERIMENTAL DETAILS

Polycrystalline samples were prepared from stoichiometric mixtures of 99.99% Ce, 99.99% Ru, 99.99% Re, and 99.999% Al by ultra high-purity argon arc melting. The crystal structure was carefully checked and refined using neutron diffraction. Magnetic susceptibility measurements were made using a Magnetic Property Measurement System (MPMS) superconducting quantum interference device (SQUID) magnetometer (Quantum Design). Electrical resistivity and heat capacity by the relaxation method were performed in a Quantum Design Physical Properties Measurement System (PPMS). The resistivity in magnetic fields up to 9 T was measured in a longitudinal configuration. Muon-spin relaxation ( $\mu\text{SR}$ ) and neutron scattering experiments were performed at the ISIS Pulsed Neutron and Muon Facility of the Rutherford Appleton Laboratory, United Kingdom. The  $\mu\text{SR}$  measurements were carried out on the MUSR spectrometer, neutron diffraction measurements on the WISH diffractometer, and inelastic neutron scattering (INS) measurements were carried out on the MARI time-of-flight (TOF) spectrometer. The  $\mu\text{SR}$  experiments were conducted in a longitudinal geometry with a powdered sample and were mounted onto a high purity silver plate. The sample and mount were then inserted into a cryostat with a temperature range of 1.2 to 300 K. In a typical  $\mu\text{SR}$  experiment almost 100% polarized positive muons are implanted in the sample where, after a short thermalization ( $<10^{-10}$  s), they start precessing about the local magnetic fields. In their decay ( $\tau = 0.2 \mu\text{s}$ ) positrons are emitted preferentially in the muon-spin direction at the instant of decay. Muons implanting into any exposed part of the silver mount give rise to a flat time independent background. The asymmetry is calculated by  $G_z(t) = [N_F(t) - \alpha N_B(t)]/[N_F(t) + \alpha N_B(t)]$ , where  $N_B(t)$  and  $N_F(t)$  are the numbers of counts at the detectors in the forward and backward positions, and  $\alpha$  is a constant determined from calibration measurements made in the paramagnetic state with a small (2 mT) applied transverse magnetic field. For the neutron diffraction experiment, a 6 g

powder sample was loaded into a cylindrical 6 mm vanadium can and placed in an Oxford Instruments cryostat. Data were recorded in the temperature interval 1.5–35 K, with long counting times (8 h) at  $T = 1.5$  and  $T = 35$  K. Intermediate temperature points were measured with a lower exposition time (2 h). The program FULLPROF [24] was used for Rietveld refinements and group theoretical calculations were performed with the aid of the ISOTROPY software [25].

## III. EXPERIMENTAL RESULTS, ANALYSES, AND DISCUSSION

### A. Magnetization, resistivity, and heat capacity

Figure 1(a) shows the magnetic susceptibility  $\chi = M/H$  vs temperature  $T$  of  $\text{CeRu}_{1.94}\text{Re}_{0.06}\text{Al}_{10}$  as measured at  $H = 1$  T in the  $T$  range 2–300 K.  $\chi(T)$  shows a broad peak at 31 K, which is well above the magnetic ordering observed through neutron diffraction and  $\mu\text{SR}$  (discussed in subsections B and C). This behavior is in contrast with the observed sharp kink in  $\chi(T)$  at 27 K (at  $T_N$ ) of  $\text{CeRu}_2\text{Al}_{10}$ , but very similar to the observed broad peak at 45 K (well above the  $T_N = 28.5$  K) in  $\text{CeOs}_2\text{Al}_{10}$  [12]. These results indicate that the

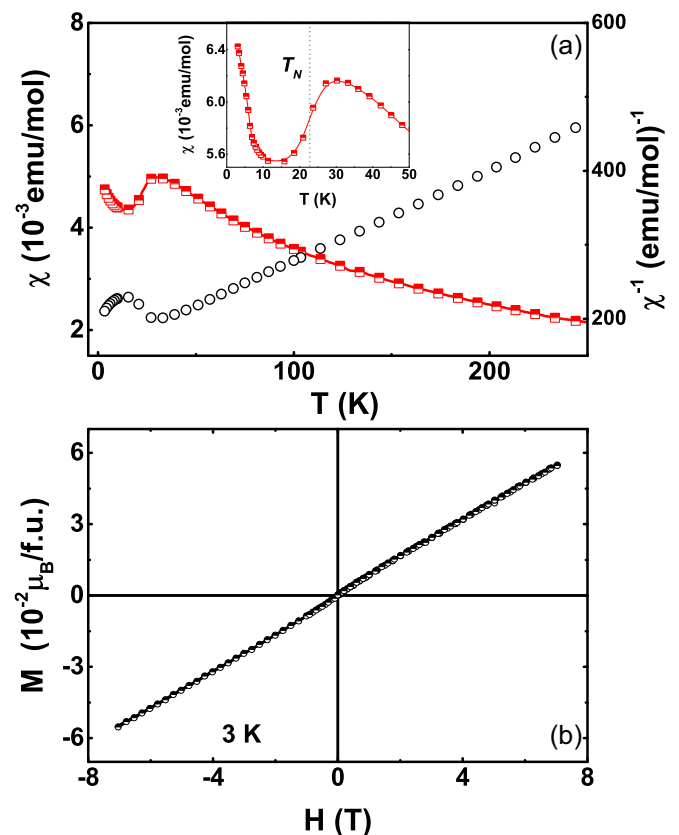


FIG. 1. (Color online) (a) Temperature dependence of the dc magnetic susceptibility ( $\chi = M/H$ ) measured in a zero field cooled condition in the presence of an applied magnetic field of 1 T for  $\text{CeRu}_{1.94}\text{Re}_{0.06}\text{Al}_{10}$ . The right scale shows the inverse dc magnetic susceptibility. The inset shows the  $\chi(T)$  data within the temperature range 2–50 K. It is clear from the  $\chi(T)$  data that the hybridization gap appears just above  $T_N$ . (b) The isothermal field dependence of magnetization at 3 K.

observed broad peak in  $\chi(T)$  at 31 K in  $\text{CeRu}_{1.94}\text{Re}_{0.06}\text{Al}_{10}$  conveys the meaning of an opening of a spin gap above  $T_N$ . The presence of a spin gap well above  $T_N$  in  $\text{CeRu}_2\text{Al}_{10}$  and  $\text{CeOs}_2\text{Al}_{10}$  has been confirmed through inelastic neutron scattering and optical measurements [12,26]. The inverse magnetic susceptibility of  $\text{CeRu}_{1.94}\text{Re}_{0.06}\text{Al}_{10}$  and likewise that of  $\text{CeRu}_2\text{Al}_{10}$  exhibits Curie-Weiss behavior above 50 K. A linear least-squares fit to the data of  $\text{CeRu}_{1.94}\text{Re}_{0.06}\text{Al}_{10}$  yields an effective magnetic moment  $p_{\text{eff}} = 2.51 \mu_B$ , which is very close to the free  $\text{Ce}^{3+}$ -ion value ( $p_{\text{eff}} = 2.54 \mu_B$ ), and a negative paramagnetic Curie temperature  $\theta_p = -100$  K. The value of the magnetic moment suggests that the Ce atoms are in their normal  $\text{Ce}^{3+}$  valence state. The negative value of  $\theta_p$  is indicative of a negative exchange constant and/or the presence of the Kondo effect. Figure 1(b) shows the  $M$  vs  $H$  isotherm recorded at 3 K.  $M$ - $H$  data imply that the net magnetization in the ordered state of  $\text{CeRu}_{1.94}\text{Re}_{0.06}\text{Al}_{10}$  is extremely low. It is far from saturation value as that expected from theoretical calculation  $gJ = 2.14 \mu_B$  for  $\text{Ce}^{3+}$  ions,  $g$  = Landé  $g$ -factor;  $J$  is the total electronic angular momentum. This is consistent with our neutron diffraction and muon-spin relaxation data presented below. The low values of the observed magnetization are expected for an AFM ground state due to the cancellation of magnetization from different magnetic sublattices of Ce ions. There is no clear sign of field induced transition for  $\text{CeRu}_{1.94}\text{Re}_{0.06}\text{Al}_{10}$  up to  $H = 7$  T. According to the magnetization which is monotonous and linear in  $H$  up to 7 T, the spontaneous AFM order remains unperturbed at this field value, which was also found in  $\text{CeRu}_2\text{Al}_{10}$  up to 13 T [27].

Figures 2(a) and 2(b) show the electrical resistivity  $\rho(T)$  of a  $\text{CeRu}_{1.94}\text{Re}_{0.06}\text{Al}_{10}$  sample in a zero field as well as the presence of various applied magnetic fields along the electrical current. The resistivity data were obtained using a standard four probe method. For  $\text{CeRu}_{1.94}\text{Re}_{0.06}\text{Al}_{10}$  the resistivity below room temperature shows activated type behavior with a narrow gap of 48 K before the onset of a sharp peak at 23 K. By fitting the  $\rho(T)$  data above  $T_N$  with the formula  $\rho = \rho_0 \exp(\Delta/2k_B T)$ ,  $k_B$  is Boltzmann constant, the value of  $\Delta/k_B$  is estimated to be 48 K. We interpret the drop in  $\rho(T)$  below its 23 K peak in terms of the antiferromagnetic spin-wave gap  $\Delta_{\text{sw}}$  expression [28]:

$$\rho(T) = \rho_0 + aT \left( 1 + \frac{2k_B T}{\Delta_{\text{sw}}} e^{-\Delta_{\text{sw}}/k_B T} \right) + AT^2. \quad (1)$$

The least-squares fit gives  $\Delta_{\text{sw}}/k_B = 39$  K,  $\rho(0) = 651 \Omega \text{ cm}$ , and  $a = 54 \Omega \text{ cm/K}$ , for the least-squares fit parameters. The Fermi liquid  $T^2$  term represents low temperature electron-electron scattering in a metal, but the  $A$  coefficient for this term turned out to be negligible in the fit. Figure 2(c) shows isothermal  $\rho$  vs  $H$  data at 2 K, 3 K, and 5 K. The magnetic field dependence of  $\rho$  is small at low magnetic fields below  $\sim 10$  T. For  $\text{CeRu}_2\text{Al}_{10}$  the magnetoresistance is small at low magnetic fields below 20 T at low temperatures,  $\rho(H)$  exhibits a negative magnetoresistance at high temperatures [29]. A negative magnetoresistance such as this is symptomatic of the conduction electron scattering by the localized magnetic moments.

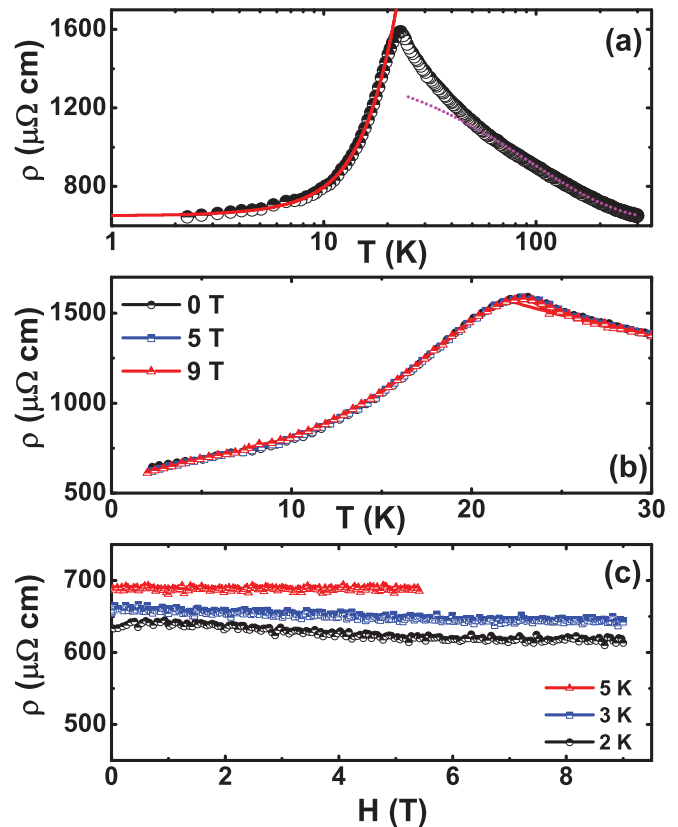


FIG. 2. (Color online) (a) Semilogarithmic plot of electrical resistivity vs temperature for  $\text{CeRu}_{1.94}\text{Re}_{0.06}\text{Al}_{10}$ . The dotted line on the high temperature data illustrates the activation type behavior of  $\rho(T)$ . Below 23 K an antiferromagnetic spin wave expression (see text) represents the data well (red line). (b) and (c) show the temperature (in the presence of various applied magnetic fields) and field dependences, respectively, of resistivity for  $\text{CeRu}_{1.94}\text{Re}_{0.06}\text{Al}_{10}$  in the longitudinal configuration.

The temperature dependence of specific heat is shown in Fig. 3(a). The midpoint (23 K) of the jump in  $C_P$  was taken as  $T_N$ . For the  $\text{CeRu}_2\text{Al}_{10}$  sample,  $C_P/T$  jumps at  $T_N$  and the extrapolation of the plot of  $C_P/T$  vs  $T^2$  to  $T = 0$  gives the Sommerfeld coefficient  $\gamma$  of  $0.246 \text{ J/K}^2 \text{ mol}$  [14]. For a small amount of hole doping ( $\text{CeRu}_{1.94}\text{Re}_{0.06}\text{Al}_{10}$ ),  $T_N$  decreases to 23 K which agrees with magnetization and  $\rho(T)$  data and jumps becomes smaller. As shown in Fig. 3(b), the specific heat above 23 K obeys  $C_P(T) = \gamma T + \beta T^2$  with  $\gamma = 0.233 \text{ J/K}^2 \text{ mol}$ . The large value of  $\gamma$  indicates that  $\text{CeRu}_{1.94}\text{Re}_{0.06}\text{Al}_{10}$  would belong to the family of heavy-fermion systems if the gap was not opened.

The excess specific heat  $\delta C_P(T) = C_P(T) - \gamma T - \beta T^2$  can be well described by a thermally activated form  $\delta C_P(T) = B \exp(-\Delta_{C_P}/T)$  with  $B = 200 \text{ J/mol K}$  and  $\Delta_{C_P} = 75 \text{ K} = 3.26 T_N$  [solid line in the inset of Fig. 3(a)]. For  $\text{CeRu}_2\text{Al}_{10}$  the relation between the energy gap and  $T_N$  is  $\Delta_{C_P} = 100 \text{ K} = 3.74 T_N$  [14]. The specific-heat data clearly reveal that the anomaly associated with the second-order phase transition ( $\lambda$  type anomaly) involves an energy gap of about 75 K. The origin of the energy gap could be either a gap over the part of the Fermi surface or an anisotropic gap in the spin wave due to a combination of single ion anisotropy and anisotropic exchange.

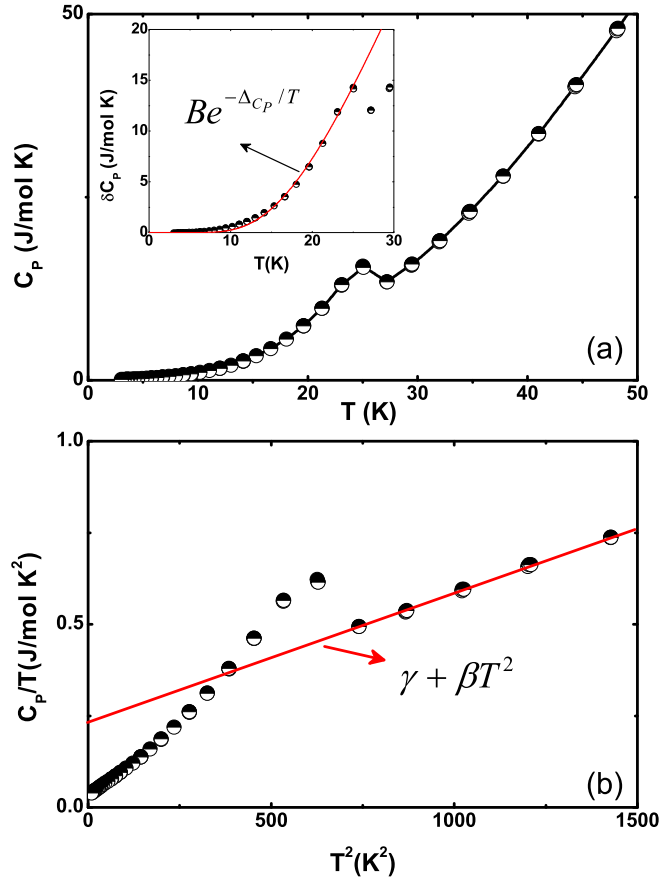


FIG. 3. (Color online) (a) Temperature variation of specific heat  $C_P$  for  $\text{CeRu}_{1.94}\text{Re}_{0.06}\text{Al}_{10}$ . The inset in (a) displays excess specific heat ( $\delta C_P$  vs  $T$ );  $\delta C_P(T) = C_P(T) - \gamma T - \beta T^3$  related to the phase transition as a function of temperature. The solid line is a fit to the data with an expression  $\delta C_P(T) = B \exp(-\Delta C_P/T)$ . (b) shows a  $C_P(T)/T$  vs  $T^2$  plots for  $\text{CeRu}_{1.94}\text{Re}_{0.06}\text{Al}_{10}$ .  $C_P(T) = \gamma T + \beta T^3$  is used to fit the experimental data above magnetic ordering.

It is noted that the extracted energy gap is also comparable to the value of the 8 meV peak from the inelastic neutron-scattering experiment. The above experimental results suggest that both  $\text{CeRu}_2\text{Al}_{10}$  and  $\text{CeRu}_{1.94}\text{Re}_{0.06}\text{Al}_{10}$  show similar phase transitions with an opening of a spin gap below  $T_N$ .

### B. Neutron diffraction: onset of magnetic long-range order

The neutron-diffraction patterns collected above 23 K (as shown in Fig. 4) for  $\text{CeRu}_{1.94}\text{Re}_{0.06}\text{Al}_{10}$  are consistent with the  $Cmcm$  symmetry of the nuclear structure and can be satisfactorily fitted with the structural model proposed by Thiede *et al.* [19,30,31]. The structural parameters are listed in Table I. Below 23 K, a set of additional weak reflections associated with the propagation vector  $\mathbf{k} = (1,0,0)$  (the Y point of symmetry in Miller and Love notations [32]) appears indicating the phase transition detected by  $\chi(T)$ ,  $\rho(T)$ ,  $C_P(T)$ , and  $\mu\text{SR}$  techniques. The origin of the transition most probably is due to a long range magnetic ordering of the Ce moments as observed in the undoped  $\text{CeRu}_2\text{Al}_{10}$  compound. This conclusion is supported by the fact that the additional reflections are only clearly visible at low-momentum transfer,

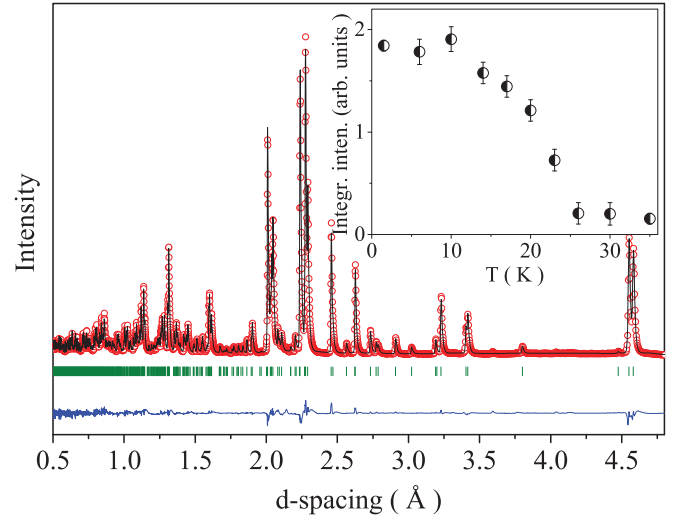


FIG. 4. (Color online) Rietveld refinement of the neutron powder diffraction pattern of  $\text{CeRu}_{1.94}\text{Re}_{0.06}\text{Al}_{10}$  ( $T = 35$  K) collected at the backscattering detectors bank (average scattering angle is  $154^\circ$ ) of the WISH diffractometer. The circle symbols (red) and solid line (black) represent the experimental and calculated intensities, respectively, and the line below (blue) is the difference between them. Tick marks indicate the positions of Bragg peaks in the  $Cmcm$  space group. The inset shows the temperature dependence of the integrated intensity of the (101) magnetic peak.

indicating that they follow the squares of the magnetic form factor  $F^2(Q)$  (here it is  $\text{Ce}^{3+}$  form factor). Another important feature is the reduction in the background observed at low  $Q$  and concomitant with the appearance of the magnetic peaks below 23 K. Once again, this is consistent with the existence of a magnetic transition below which the intensity contained in the paramagnetic scattering is suppressed and transferred to magnetic Bragg scattering. The temperature dependence of the integrated intensity of the strongest (101) magnetic Bragg peak is shown in Fig. 4 (inset).

TABLE I. Structural parameters of  $\text{CeRu}_{1.94}\text{Re}_{0.06}\text{Al}_{10}$  refined from the neutron diffraction data collected at  $T = 35$  K in the orthorhombic  $Cmcm$  ( $R_{\text{bragg}} = 3.98\%$ ) space group. Occupancies for all the atoms in the refinement procedure were fixed to the nominal chemical content.

Atom	Site	$x$	$y$	$z$
Ce	4c	0	0.1265(3)	0.25
Ru/Re	8d	0.25	0.25	0
Al1	8g	0.2237(3)	0.3625(1)	0.25
Al2	8g	0.3490(2)	0.1314(3)	0.25
Al3	8f	0	0.1616(4)	0.5986(4)
Al4	8f	0	0.3796(3)	0.0496(1)
Al5	8e	0.2291(3)	0	0
$\text{Ce}(\text{Ru}_{1-x}$	$a$	$b$	$c$	$V$
$\text{Re}_x)_2\text{Al}_{10}$	(Å)	(Å)	(Å)	(Å <sup>3</sup> )
$x = 0$	9.1322(2)	10.2906(1)	9.1948(2)	864.08
$x = 0.03$	9.1292(2)	10.2870(1)	9.1914(2)	863.185

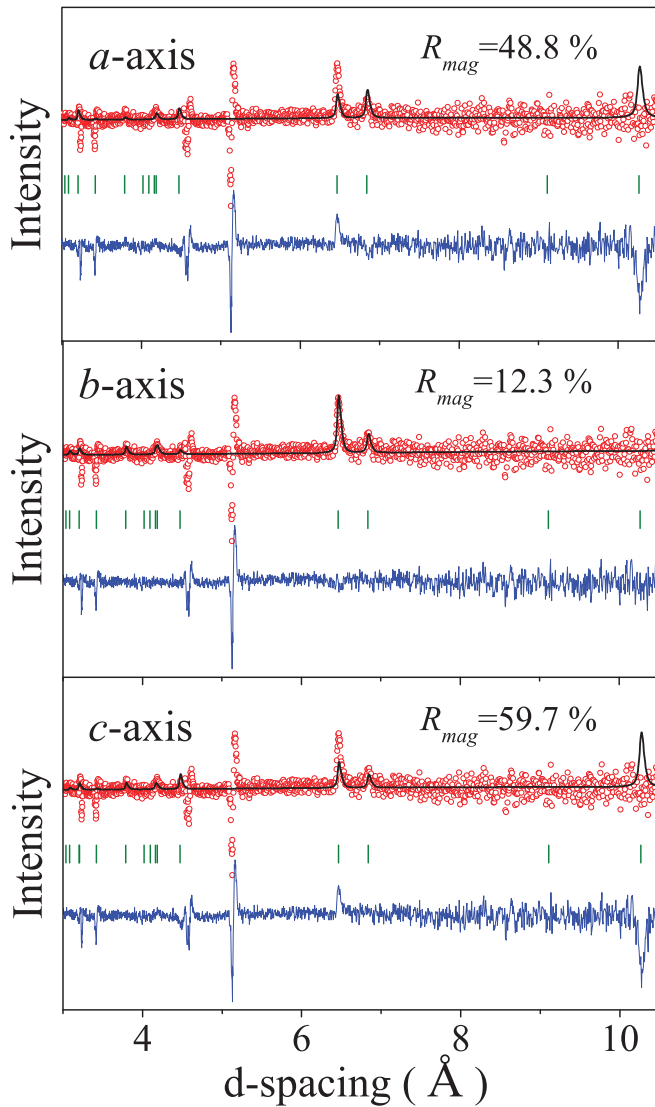


FIG. 5. (Color online) Rietveld refinements of the magnetic intensity of the  $\text{CeRu}_{1.94}\text{Re}_{0.06}\text{Al}_{10}$  composition obtained as a difference between the diffraction patterns collected at 1.5 and 35 K. The circle symbols (red) and solid line represent the experimental and calculated intensities, respectively, and the line below (blue) is the difference between them. Tick marks indicate the positions of Bragg peaks for the magnetic scattering with the ( $\mathbf{k} = 1,0,0$ ) propagation vector. The refinement quality is demonstrated for three models, with moments along the  $a$  axis (top),  $b$  axis (middle), and  $c$  axis (bottom). The asymmetric features are due to slight differences in the  $d$  spacing of the nuclear peaks at different temperatures (thermal expansion).

By taking the difference between the diffraction patterns collected at  $T = 1.5$  and  $T = 35$  K, several magnetic Bragg peaks with intensities significantly higher than the error bars (Fig. 5) can be identified. The important observation from the difference plot is the absence of the magnetic (010) peak near  $10.3 \text{ \AA}$ , which is clearly seen in pure  $\text{CeRu}_2\text{Al}_{10}$ ,  $\text{Ce}(\text{Ru}_{1-x}\text{Fe}_x)_2\text{Al}_{10}$ ,  $x = 0.4$ , and  $\text{CeOs}_2\text{Al}_{10}$  [16,19,20]. Taking into account that neutron scattering intensity is proportional to the square of the moment component perpendicular to the scattering vector, this observation confirms that the magnetic moment direction in  $\text{CeRu}_{1.94}\text{Re}_{0.06}\text{Al}_{10}$  is along

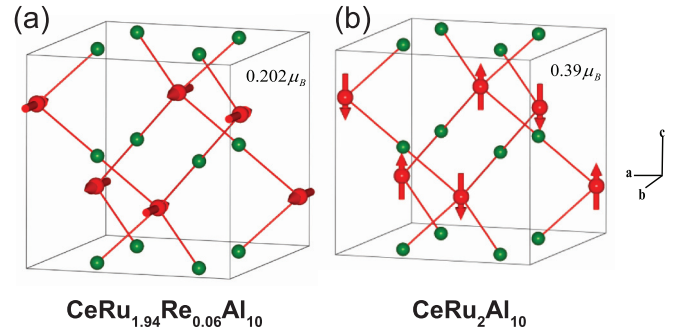


FIG. 6. (Color online) Magnetic structures of the hole-doped (found in this paper) and  $\text{CeRu}_2\text{Al}_{10}$  [19] samples. For clarity, only Ce (red) and Ru/Re (green) atoms are shown.

the  $b$  axis and not along  $c$  axis as observed in  $\text{CeRu}_2\text{Al}_{10}$ ,  $\text{CeOs}_2\text{Al}_{10}$ , and  $\text{CeOs}_{1.94}\text{Re}_{0.06}\text{Al}_{10}$  [23]. Further it is to be noted that the moment direction in  $\text{Ce}(\text{Os}_{1-x}\text{Ir}_x)_2\text{Al}_{10}$ ,  $x = 0.08$ , is along the  $a$  axis [moment value of  $0.92(1) \mu_B$ ] [34]. In spite of the different moment direction, the observed magnetic Bragg peaks in  $\text{CeRu}_{1.94}\text{Re}_{0.06}\text{Al}_{10}$  can be indexed based on the propagation vector  $\mathbf{k} = (1,0,0)$ , which is the same as observed in pure  $\text{CeRu}_2\text{Al}_{10}$  [19].

To obtain an appropriate model for the magnetic structure of  $\text{CeRu}_{1.94}\text{Re}_{0.06}\text{Al}_{10}$ , we employed a method whereby combinations of axial vectors localized on the  $4c(\text{Ce})$  site and transforming as basis functions of the irreducible representations of the wave-vector group [ $\mathbf{k} = (1,0,0)$ ] are systematically tested [35]. The symmetry analysis reveals that the reducible magnetic representation is decomposed into six one-dimensional representations, labeled  $Y_i^+$  ( $i = 2,3,4$ ) and  $Y_i^-$  ( $i = 1,2,3$ ). The  $Y_i^+$  representations imply ferromagnetic (FM) alignment of the Ce moments within the primitive unit cell, along different crystallographic directions. On the other hand,  $Y_i^-$  transform Ce moments which are AFM coupled within the primitive unit cell. In agreement with the Landau theory of continuous transitions, we found that a single irreducible representation is involved. A unique solution associated with the  $Y_1^-$  representation was found to provide an excellent refinement quality of the magnetic intensity [Fig. 5 (middle)]. The refinement yields the ordered state of Ce moments along the  $b$  axis to be  $0.20(1) \mu_B$  [see Fig. 6(a), where the magnetic unit cell is shown]. On the other hand the fit to the data with the moments along either the  $a$  axis [Fig. 5 (top)] or the  $c$  axis [Fig. 5 (bottom)] results in a much worse refinement quality. Thus, there are two important differences to be noted compared with the parent  $\text{CeRu}_2\text{Al}_{10}$ : (1) the ordered moments value is almost half in the present sample compared to the undoped one and (2) the direction of the moments is along the  $b$  axis and not along the  $c$  axis as in undoped  $\text{CeRu}_2\text{Al}_{10}$  and also in  $\text{CeOs}_{1.94}\text{Re}_{0.06}\text{Al}_{10}$  [19,23]; see Fig. 6(b).

### C. Muon-spin relaxation: evidence of a small magnetic moment in the ordered state

To investigate the microscopic magnetic nature at  $T_N$  we have measured positive muon-spin relaxation on  $\text{CeRu}_{1.94}\text{Re}_{0.06}\text{Al}_{10}$ , using polycrystalline samples in the temperature range between 1.5 and 50 K. The  $\mu\text{SR}$  technique is

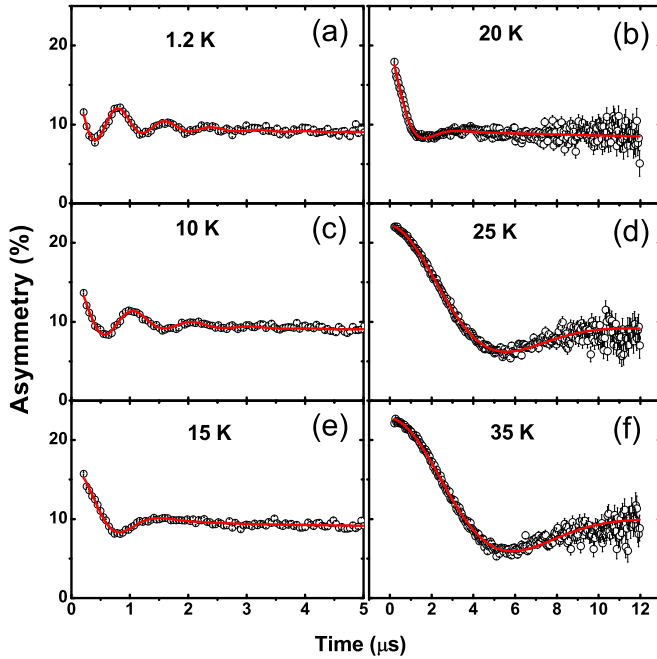


FIG. 7. (Color online) The time evolution of the muon-spin relaxation for various temperatures (above and below  $T_N$ ) in a zero field. The solid lines are least-squares fits [using Eq. (2) (above  $T_N$ ) and Eq. (3) (below  $T_N$ )] to the data as described in the text.

sensitive to local magnetic order via the decrease in muon asymmetry spectra and the enhanced muon-spin relaxation at the transition temperature. For  $\text{CeRu}_2\text{Al}_{10}$  two muon frequencies (10.5 and 3 mT) were observed, suggesting that muons occupy at least two different sites in the sample [19]. One of these components also exhibits unusual behaviors, showing a dip at about 11 K in the temperature dependence, and was suggested to be probably related to a structure distortion or resistivity anomaly. For  $\text{CeRu}_{1.94}\text{Re}_{0.06}\text{Al}_{10}$  we found Kubo-Toyabe type behavior above  $T_N$  (like  $\text{CeRu}_2\text{Al}_{10}$ ), and below  $T_N$  it shows a clear signature of time oscillation consistent with a very small ordered moment  $0.20(1) \mu_B$ .

Detailed  $\mu\text{SR}$  data were obtained in zero external field in order to study the variation of  $B_{\text{int}}$  with  $T$ . Figures 7(a)–7(f) show the zero-field time dependence asymmetry spectra at various temperatures below and above magnetic ordering temperature of  $\text{CeRu}_{1.94}\text{Re}_{0.06}\text{Al}_{10}$ . It is clear from Fig. 7 that a small amount of hole doping drastically changes the time dependence of asymmetry spectra compared with the pure compound. Above 23 K, we observe Kubo-Toyabe (KT) type behavior [36], i.e., a strong damping at shorter time and the recovery at longer times, arising from a static distribution of the nuclear dipole moment. On the time scale of the muon, these nuclear spins are static and randomly orientated. The spectra above the phase transition temperature are best described by Kubo-Toyabe times exponential decay function plus a constant background term given below [fits are shown in Figs. 7(d) and 7(f)]:

$$G_{z1}^{\text{KT}}(t) = \frac{A_2}{3} \left[ 1 + 2(1 - \sigma_{\text{KT}}^2 t^2) e^{-\frac{\sigma_{\text{KT}}^2 t^2}{2}} \right] e^{-\lambda_2 t} + A_{\text{bg}}, \quad (2)$$

where initial amplitude of the KT decay is  $A_2$ ;  $\lambda_2$  is the relaxation rate associated with the dynamic electronic spin

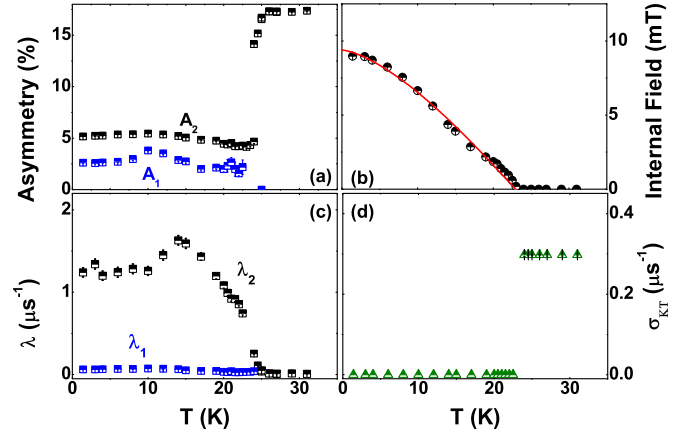


FIG. 8. (Color online) The temperature dependence of (a) the initial asymmetries  $A_1$  and  $A_2$ , (b) the internal field at the muon site, (c) the depolarization rates  $\lambda_1$  and  $\lambda_2$ , and (d) the depolarization rate  $\sigma_{\text{KT}}$ . The solid line in (b) is fit to the data using Eq. (4) (see text).

fluctuations;  $A_{\text{bg}}$  is a constant background arising from muon stopping on the silver sample holder.  $A_{\text{bg}}$  was estimated from 50 K data and kept fixed for fitting all the other spectra. The nuclear depolarization rate is  $\sigma_{\text{KT}}$ , and  $\sigma_{\text{KT}}/\gamma_\mu = \Delta$  is the local Gaussian field distribution width;  $\gamma_\mu$  is the gyromagnetic ratio of the muon.  $\sigma_{\text{KT}}$  was found to be almost temperature independent as shown in Fig. 8(d) with its value equal to  $0.29 \mu\text{s}^{-1}$ . Using a similar  $\sigma_{\text{KT}}$  value, Kambe *et al.* [37] have suggested  $4a$  (0,0,0) as the muon stopping site in  $\text{CeRu}_2\text{Al}_{10}$ , while for  $\text{CeOs}_2\text{Al}_{10}$  [33,38], the muon stopping site was assigned to the  $4c$  (0.5,0,0.25) position. The dipolar fields calculation by Guo *et al.* on  $\text{Ce}(\text{Ru}_{1-x}\text{Rh}_x)_2\text{Al}_{10}$  ( $x = 0-0.08$ ) [39] suggest two stopping sites  $4c$  and  $4a$ , in the latter, the internal field is almost zero. Our dipolar fields calculation for  $\text{CeRu}_{1.94}\text{Re}_{0.06}\text{Al}_{10}$  suggest a muon stopping site is  $4c$  (0.5,0,0.25).

As the temperature is approached near magnetic transition, the  $\mu\text{SR}$  spectra clearly show the presence of coherent oscillations. Below 23 K, all spectra are well described uniformly by the phenomenological function

$$G_{z2}(t) = A_1 \cos(\omega t + \phi) e^{-\lambda_1 t} + G_{z1}^{\text{KT}}(t), \quad (3)$$

where  $\sigma_{\text{KT}} = 0$ , the  $G_{z1}^{\text{KT}}(t)$  term becomes  $A_2 e^{-\lambda_2 t} + A_{\text{bg}}$ ,  $\lambda_1$  is the muon depolarization rate (arising from the distribution of the internal field),  $\phi$  is the phase, and  $\omega = \gamma_\mu B_{\text{int}}$  is the muon precession frequency ( $B_{\text{int}}$  is the internal field at the muon site). The first term represents the transverse components of the internal fields seen by the muons along which they precess, while the second term represents the longitudinal component.

The temperature dependencies of these parameters are shown in Figs. 8(a)–8(d). Below 23 K, as shown in Fig. 8(a) there is a loss of initial asymmetry in  $A_2$  compared to that of the high temperature value. The initial asymmetry associated with frequency term  $A_1$  starts to increase below this temperature (23 K) [see Fig. 8(a)], indicating the onset of a long-range ordered state in  $\text{CeRu}_{1.94}\text{Re}_{0.06}\text{Al}_{10}$  which agrees with the specific heat and magnetic susceptibility data. The value of the Lorentzian decay term  $\lambda_2$  starts to increase below 23 K.  $\lambda_1$  associated with oscillating term on

the other hand remains almost constant. Figure 8(d) shows the temperature dependence of the muon depolarization rate which seems temperature independent above  $T_N$ . Figure 8(b) shows the temperature dependence of the internal field (or muon precession frequency) at the muon site. This shows that the internal fields appear below 23 K, signifying clear evidence for long-range magnetic order. However, the associated internal fields are found to be the same order of magnitude compared to  $\text{CeRu}_2\text{Al}_{10}$  ( $B_{\text{int}} = 10$  mT at base temperature). In order to find out the nature of the magnetic interaction, the temperature dependence of internal field was fitted [40]:

$$B_{\text{int}}(T) = B_0 \left[ 1 - \left( \frac{T}{T_N} \right)^\alpha \right]^\beta. \quad (4)$$

Observed parameters are  $\beta = 0.96(2)$ ,  $B_0 = 9.4(3)$  mT,  $\alpha = 1.47(2)$ , and  $T_N = 23(3)$  K. A fit with  $\beta \sim 0.96(2)$  suggests the magnetic interactions in the hole-doped system is non-mean-field-like behavior.  $\alpha > 1$  indicates complex magnetic interactions in this system [41,42].

#### D. Inelastic neutron scattering study

INS measurements on  $\text{CeRu}_2\text{Al}_{10}$  clearly revealed the presence of a sharp inelastic magnetic excitation near 8 meV below 29 K, due to the opening of a gap in the spin-excitation spectrum, which transforms into a broad response at and above 35 K [31,33]. Hole doping results in a dramatic change in magnetic moment directions and its value is reduced to almost half compared to the undoped system. It is of great interest to study inelastic neutron scattering to see how the spin gap and its  $Q$  and temperature dependencies vary for  $\text{CeRu}_{1.94}\text{Re}_{0.06}\text{Al}_{10}$ . In this subsection we briefly report on the temperature dependence of low energy INS spectra of  $\text{CeRu}_{1.94}\text{Re}_{0.06}\text{Al}_{10}$ . We have also measured the nonmagnetic phonon reference compound  $\text{LaRu}_2\text{Al}_{10}$ .

Figures 9(a)–9(c) show the color plots of the total scattering intensity (magnetic and phonon contributions), energy transfer vs momentum transfer measured at 5 K for  $\text{CeRu}_2\text{Al}_{10}$ ,  $\text{CeRu}_{1.94}\text{Re}_{0.06}\text{Al}_{10}$ , and  $\text{LaRu}_2\text{Al}_{10}$ . For the  $\text{CeRu}_{1.94}\text{Re}_{0.06}\text{Al}_{10}$  compound we find clear magnetic excitation or spin gap energy around 8 meV. This value is in agreement with the spin gap energy estimated from the specific heat and resistivity studies as discussed earlier. Further for comparison we have also shown the scattering from the nonmagnetic reference compound  $\text{LaRu}_2\text{Al}_{10}$  which confirms the magnetic nature of the excitations in the Ce compounds. We have plotted the data in one-dimensional (1D) ( $Q$  integrated between 0 and 2.5 Å) energy cuts [see Figs. 10(a)–10(c)] taken from the two-dimensional (2D) plots. It is clear from these 1D cuts that the position of the spin gap excitation remains nearly the same in both the compounds while the linewidth of the excitation increases in the Re-doped systems:  $\Gamma = 1.1$  for  $\text{CeRu}_2\text{Al}_{10}$  and 1.6 meV for  $\text{CeRu}_{1.94}\text{Re}_{0.06}\text{Al}_{10}$ . The estimated value of the susceptibility ( $\chi_{\text{INS}}$ ) at 5 K is  $3.6 \times 10^{-3}$  for  $\text{CeRu}_{1.94}\text{Re}_{0.06}\text{Al}_{10}$  and  $5.1 \times 10^{-3}$  emu/mol for  $\text{CeRu}_2\text{Al}_{10}$ . At 25 and 35 K the excitation becomes broad, but still keep its inelastic nature.

Now we compare the effect of the reduction of the moment and its direction on the stability of the spin gap type excitations in the doped  $\text{CeRu}_2\text{Al}_{10}$  and  $\text{CeOs}_2\text{Al}_{10}$ . First we would

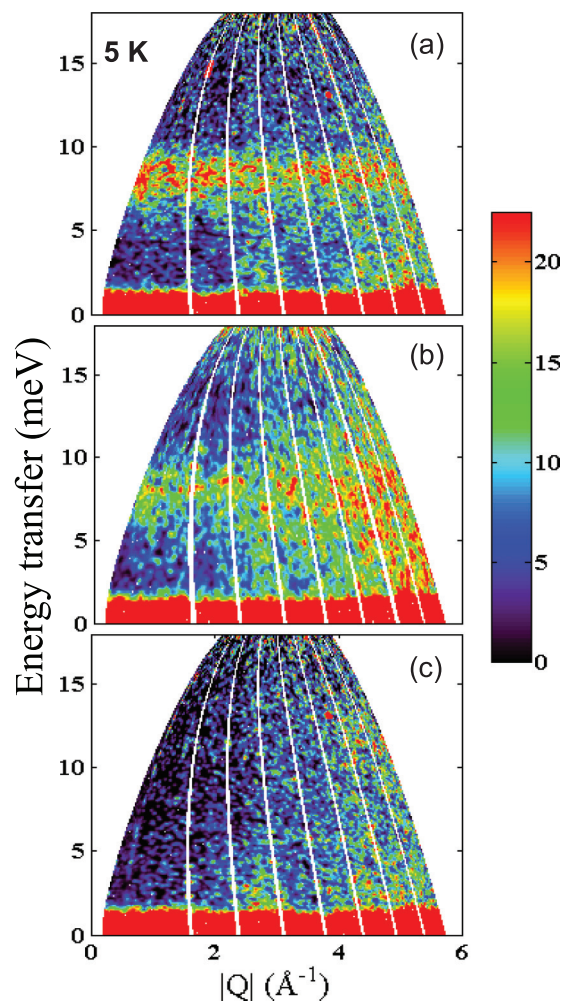


FIG. 9. (Color online) Color-coded inelastic neutron scattering intensity of (a)  $\text{CeRu}_2\text{Al}_{10}$ , (b)  $\text{CeRu}_{1.94}\text{Re}_{0.06}\text{Al}_{10}$ , and (c) nonmagnetic  $\text{LaRu}_2\text{Al}_{10}$ , at 5 K, measured with an incident energy of  $E_i = 20$  meV on the MARI spectrometer.

like to mention that in the present case for both doped ( $\text{CeRu}_{1.94}\text{Re}_{0.06}\text{Al}_{10}$ ) and undoped ( $\text{CeRu}_2\text{Al}_{10}$ ) systems the moment direction does not align along the CEF anisotropy, which expects a moment along the  $a$  axis, and further the observed moment values are reduced considerably from the free-ion Hund's rule values,  $0.20(1) \mu_B$  and  $0.34\text{--}0.42 \mu_B$ , respectively. For the results of these, we have seen well defined spin gap excitations in both the systems having a small moment that does not follow CEF anisotropy. Our preliminary measurements of inelastic neutron scattering on electron doped (i.e., 10% Rh) in  $\text{CeRu}_2\text{Al}_{10}$  reveals that the spin gap value is reduced to 5 meV at 5 K with a considerable reduction in the intensity with a broadened linewidth, which make it difficult to detect the spin gap clearly [43]. The study of  $\mu\text{SR}$  on  $\text{Ce}(\text{Ru}_{1-x}\text{Rh}_x)_2\text{Al}_{10}$  clearly indicates that the internal fields are higher in the Rh-doped samples [39], which directly implies a larger moment value, which has been also confirmed by a recent neutron diffraction study [44]. A very similar increase in the moment value,  $1 \mu_B$ , with the direction of the moment along the  $a$  axis has been observed in  $\text{Ce}(\text{Os}_{1-x}\text{Ir}_x)_2\text{Al}_{10}$ , and an inelastic study in this case does not reveal any sign of a

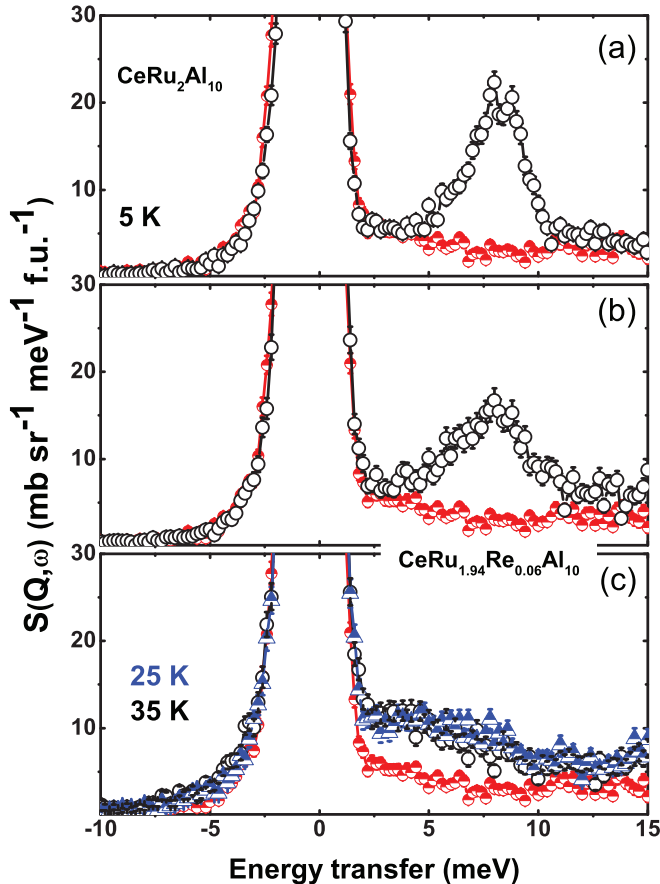


FIG. 10. (Color online)  $Q$ -integrated ( $0 \leq Q \leq 2.5 \text{ \AA}$ ) intensity vs energy transfer of (a)  $\text{CeRu}_2\text{Al}_{10}$  and (b), (c)  $\text{CeRu}_{1.94}\text{Re}_{0.06}\text{Al}_{10}$  along with the nonmagnetic phonon reference compound  $\text{LaRu}_2\text{Al}_{10}$  (red half filled circles), measured with an incident energy of  $E_i = 20 \text{ meV}$ .

spin gap down to 2 K and also down to 0.6 meV [38]. These observations indicate that when the ordered state moment value is larger that destabilizes the spin gap formation. This implies that when the ordered moment value is small, and moreover not aligned with the CEF easy axis, then the  $c$ - $f$  hybridization is active and stabilizes the spin gap, while when the moment value is larger (and follows CEF anisotropy) the spin gap becomes unstable.

### E. Concluding remarks

Our results provide compelling evidence that the  $\text{CeRu}_{1.94}\text{Re}_{0.06}\text{Al}_{10}$  exhibits a phase transition at 23 K associated with long-range magnetic ordering of the Ce sublattice. The propagation vector of the ordered state is  $\mathbf{k} = (1,0,0)$  and it does not change with temperature. The magnetic structure at  $T = 1.5 \text{ K}$  involves a collinear antiferromagnetic orientation of the Ce moments along the  $b$  axis of the  $Cmcm$  space group with a magnitude of  $0.20(1) \mu_B$ .

Further inelastic neutron scattering study reveals a clear sign of the spin gap type excitation with an energy scale of 8 meV in the hole-doped system, which is the same as that observed in the undoped  $\text{CeRu}_2\text{Al}_{10}$ . Our present hole doping study along with other investigations on the doped systems of  $\text{CeT}_2\text{Al}_{10}$  ( $T = \text{Ru}$  and  $\text{Os}$ ) indicate that the smaller value of the ordered state moment (also the direction not governed by CEF anisotropy) stabilizes the spin gap formation. On the other hand the larger value ( $\sim 1 \mu_B$ ) of the ordered state moment (governed by CEF anisotropy) destabilizes the spin gap ground state. It has been reported through magnetization study that the ordered state moment is along the  $b$  axis in  $\text{Ce}_{1-x}\text{La}_x\text{Ru}_2\text{Al}_{10}$  ( $x = 0.1$ ) at ambient pressure. This has been attributed to a negative chemical pressure effect [45]. However, in the present hole-doped study the volume contracts by 0.1%, concomitant with a positive chemical pressure. Considering these two observations we propose that change in the moment direction in the hole-doped  $\text{CeRu}_2\text{Al}_{10}$  is due to an electronic effect. It is expected that our findings in this work will generate new theoretical interest that might help one to understand the real mechanism of spin gap formation and the higher magnetic ordering temperature of this family of compounds.

### ACKNOWLEDGMENTS

We would like to thank Professor P. Riseborough, Dr. Jean-Michel Mignot, and Professor Y. Muro for an interesting discussion. A.B. would like to acknowledge FRC of UJ, NRF of South Africa, and ISIS-STFC for funding support. D.T.A. and A.D.H. thank the CMPC-STFC, Grant No. CMPC-09108, for financial support. A.M.S. thanks the SA-NRF (Grant No. 78832) and UJ Research Committee for financial support. T.T. thanks KAKENHI No. 26400363 from MEXT, Japan.

- [1] A. C. Hewson, *The Kondo Problem to Heavy Fermions* (Cambridge University Press, Cambridge, 1993).
- [2] J. W. Allen, B. Batlogg, and P. Wachter, *Phys. Rev. B* **20**, 4807 (1979).
- [3] M. Kasaya, F. Iga, K. Negishi, S. Nakai, and T. Kasuya, *J. Magn. Magn. Mater* **31–34**, 437 (1983).
- [4] T. Takabatake, F. Iga, T. Yoshino, Y. Echizen, K. Katoh, K. Kobayashi, M. Higa, N. Shimizu, Y. Bando, G. Nakamoto, H. Fujii, K. Izawa, T. Suzuki, T. Fujita, M. Sera, M. Hiroi, K. Maezawa, S. Mock, H. v. Löhneysen, A. Brückl, K. Neumaier, and K. Andres, *J. Magn. Magn. Mater.* **177**, 277 (1998).
- [5] S. Yoshii, M. Kasaya, H. Takahashi, and N. Mori, *Physica B* **223**, 421 (1996).
- [6] K. Umeo, T. Igaue, H. Chyono, Y. Echizen, T. Takabatake, M. Kosaka, and Y. Uwatoko, *Phys. Rev. B* **60**, R6957 (1999).
- [7] Y. Uwatoko, N. Mori, G. Oomi, and J. D. Thompson, *Physica B* **239**, 95 (1997).
- [8] T. Sasakawa, H. Miyaoka, K. Umeo, S. Aoyagi, K. Kato, F. Iga, and T. Takabatake, *J. Phys. Soc. Jpn.* **73**, 262 (2004).
- [9] L. Degiorgi, *Rev. Mod. Phys.* **71**, 687 (1999).
- [10] P. S. Riseborough, *Adv. Phys.* **49**, 257 (2000).
- [11] A. M. Strydom, *Physica B* **404**, 2981 (2009).
- [12] D. T. Adroja, A. D. Hillier, Y. Muro, T. Takabatake, A. M. Strydom, A. Bhattacharyya, A. Daoud-Aladin, and J. W. Taylor, *Phys. Scr.* **88**, 068505 (2013).



- [13] T. Nishioka, Y. Kawamura, T. Takesaka, R. Kobayashi, H. Kato, M. Matsumura, K. Kodama, K. Matsubayashi, and Y. Uwatoko, *J. Phys. Soc. Jpn.* **78**, 123705 (2009).
- [14] C. S. Lue, S. H. Yang, A. C. Abhyankar, Y. D. Hsu, H. T. Hong, and Y. K. Kuo, *Phys. Rev. B* **82**, 045111 (2010).
- [15] D. T. Adroja, A. D. Hillier, Y. Muro, J. Kajino, T. Takabatake, P. Peratheepan, A. M. Strydom, P. P. Deen, F. Demmel, J. R. Stewart, J. W. Taylor, R. I. Smith, S. Ramos, and M. A. Adams, *Phys. Rev. B* **87**, 224415 (2013).
- [16] J. Robert, J.-M. Mignot, S. Petit, P. Steffens, T. Nishioka, R. Kobayashi, M. Matsumura, H. Tanida, D. Tanaka, and M. Sera, *Phys. Rev. Lett.* **109**, 267208 (2012).
- [17] S. Kimura, T. Iizuka, Y. Muro, J. Kajino, and T. Takabatake, *J. Phys.: Conf. Ser.* **391**, 012030 (2012).
- [18] A. Slebarski and J. Goraus, *J. Phys.: Conf. Ser.* **391**, 012067 (2012).
- [19] D. D. Khalyavin, A. D. Hillier, D. T. Adroja, A. M. Strydom, P. Manuel, L. C. Chapon, P. Peratheepan, K. Knight, P. Deen, C. Ritter, Y. Muro, and T. Takabatake, *Phys. Rev. B* **82**, 100405(R) (2010).
- [20] H. Kato, R. Kobayashi, T. Takesaka, T. Nishioka, M. Matsumura, K. Kaneko, and N. Metoki, *J. Phys. Soc. Jpn.* **80**, 073701 (2011).
- [21] T. Takesaka, K. Oe, R. Kobayashi, Y. Kawamura, T. Nishioka, H. Kato, M. Matsumura, and K. Kodama, *J. Phys.: Conf. Ser.* **200**, 012201 (2010).
- [22] V. Guritanu, P. Wissgott, T. Weig, H. Winkler, J. Sichelschmidt, M. Scheffler, A. Prokofiev, S. Kimura, T. Iizuka, A. M. Strydom, M. Dressel, F. Steglich, K. Held, and S. Paschen, *Phys. Rev. B* **87**, 115129 (2013).
- [23] D. D. Khalyavin, D. T. Adroja, A. Bhattacharyya, A. D. Hillier, P. Manuel, A. M. Strydom, J. Kawabata, and T. Takabatake, *Phys. Rev. B* **89**, 064422 (2014).
- [24] J. Rodríguez-Carvajal, *Physica B* **192**, 55 (1993).
- [25] H. T. Stokes, D. M. Hatch, and B. J. Campbell, ISOTROPY, [stokes.byu.edu/isotropy.html](http://stokes.byu.edu/isotropy.html) (2007); B. J. Campbell, H. T. Stokes, D. E. Tanner, and D. M. Hatch, *J. Appl. Crystallogr.* **39**, 607 (2006).
- [26] S.-i. Kimura, T. Iizuka, H. Miyazaki, A. Irizawa, Y. Muro, and T. Takabatake, *Phys. Rev. Lett.* **106**, 056404 (2011).
- [27] A. M. Strydom, *J. Low Temp Phys.* **159**, 160 (2010).
- [28] N. Hessel Andersen, in *Crystalline Electric Field and Structural Effects in f-Electron Systems*, edited by J. E. Crow, P. Guertin, and T. W. Mihalisin (Plenum, New York, 1980), p. 273.
- [29] A. Kondo, J. Wang, K. Kindo, T. Takesaka, Y. Ogane, Y. Kawamura, T. Nishioka, D. Tanaka, H. Tanida, and M. Sera, *J. Phys. Soc. Jpn.* **80**, 013701 (2011).
- [30] V. M. T. Thiede, T. Ebel, and W. Jeitschko, *J. Mater. Chem.* **8**, 125 (1998).
- [31] J. Robert, J.-M. Mignot, G. André, T. Nishioka, R. Kobayashi, M. Matsumura, H. Tanida, D. Tanaka, and M. Sera, *Phys. Rev. B* **82**, 100404(R) (2010).
- [32] S. C. Miller and W. F. Love, *Tables of Irreducible Representations of Space Groups and Co-Representations of Magnetic Space Groups*, 4th ed. (Preutt Press, Boulder, 1967).
- [33] D. T. Adroja, A. D. Hillier, P. P. Deen, A. M. Strydom, Y. Muro, J. Kajino, W. A. Kockelmann, T. Takabatake, V. K. Anand, J. R. Stewart, and J. Taylor, *Phys. Rev. B* **82**, 104405 (2010).
- [34] D. D. Khalyavin, D. T. Adroja, P. Manuel, J. Kawabata, K. Umeo, T. Takabatake, and A. M. Strydom, *Phys. Rev. B* **88**, 060403 (2013).
- [35] Yu. A. Izumov, V. E. Naish, and R. P. Ozerov, *Neutron Diffraction of Magnetic Materials* (Consulting Bureau, New York, 1991).
- [36] R. S. Hayano, Y. J. Uemura, J. Imazato, N. Nishida, T. Yamazaki, and R. Kubo, *Phys. Rev. B* **20**, 850 (1979).
- [37] S. Kambe, H. Chudo, Y. Takunaga, T. Koyama, H. Sakai, T. U. Ito, K. Ninomiya, W. Higemoto, T. Takesaka, T. Nishioka, and Y. Miyake, *J. Phys. Soc. Jpn.* **79**, 053708 (2010).
- [38] A. Bhattacharyya, D. T. Adroja, A. M. Strydom, J. Kawabata, T. Takabatake, A. D. Hillier, V. Garcia Sakai, J. W. Taylor, and R. I. Smith, [arXiv:1407.2516](https://arxiv.org/abs/1407.2516) [Phys. Rev. B (to be published)].
- [39] H. Guo, H. Tanida, R. Kobayashi, I. Kawasaki, M. Sera, T. Nishioka, M. Matsumura, I. Watanabe, and Z. A. Xu, *Phys. Rev. B* **88**, 115206 (2013).
- [40] A. Bhattacharyya, D. T. Adroja, A. M. Strydom, A. D. Hillier, J. W. Taylor, A. Thamizhavel, S. K. Dhar, W. A. Kockelmann, and B. D. Rainford, *Phys. Rev. B* **90**, 054405 (2014).
- [41] D. I. Khomskii, *Basic Aspects of the Quantum Theory of Solids: Order and Elementary Excitations* (Cambridge University Press, Cambridge, 2010).
- [42] S. Blundell, *Magnetism in Condensed Matter*, Oxford Master Series in Condensed Matter (Oxford University Press, Oxford, 2001).
- [43] D. T. Adroja, A. Bhattacharyya, A. M. Strydom *et al.* (unpublished); J.-M. Mignot and J. Robert (private communication, 2014).
- [44] R. Kobayashi, K. Kaneko, K. Saito, J.-M. Mignot, G. André, J. Robert, S. Wakimoto, M. Matsuda, S. Chi, Y. Haga, T. D. Matsuda, E. Yamamoto, T. Nishioka, M. Matsumura, H. Tanida, and M. Sera, *J. Phys. Soc. Jpn.* **83**, 104707 (2014).
- [45] H. Tanida, D. Tanaka, Y. Nonaka, S. Kobayashi, M. Sera, T. Nishioka, and M. Matsumura, *Phys. Rev. B* **88**, 045135 (2013).